In vivo evaluation of [11C]preladenant positron emission tomography for quantification of adenosine A_{2A} receptors in the rat brain

Xiaoyun Zhou, Shivashankar Khanapur, Johan R de Jong, Antoon TM Willemsen, Rudi AJO Dierckx, Philip H Elsinga and Erik FJ de Vries

Abstract

[11C]Preladenant was developed as a novel adenosine A_{2A} receptor positron emission tomography radioligand. The present study aims to evaluate the suitability of [11C]preladenant positron emission tomography for the quantification of striatal A_{2A} receptor density and the assessment of striatal A_{2A} receptor occupancy by KW-6002. Sixty- or ninety-minute dynamic positron emission tomography imaging was performed on rats. Tracer kinetics was quantified by the two-tissue compartment model, Logan graphical analysis and several reference tissue-based models. Test–retest reproducibility was assessed by repeated imaging on two consecutive days. Two-tissue compartment model and Logan plot estimated comparable distribution volume (V_T) values of ∼10 in the A_{2A} receptor-rich striatum and substantially lower values in all extra-striatal regions (∼1.5–2.5). The simplified reference tissue model with midbrain or occipital cortex as the reference region proved to be the best non-invasive model for quantification of A_{2A} receptor, showing a striatal binding potential (BP_{ND}) value of ∼5.5, and a test–retest variability of ∼5.5%. The brain metabolite analysis showed that at 60-min post injection, 17% of the radioactivity in the brain was due to radioactive metabolites. The ED_{50} of KW-6002 in rat striatum for i.p. injection was 0.044–0.062 mg/kg. The study demonstrates that [11C]preladenant is a suitable tracer to quantify striatal A_{2A} receptor density and assess A_{2A} receptor occupancy by A_{2A} receptor-targeting molecules.

Introduction

Adenosine is a signaling molecule that functions via activation of four subtypes of adenosine receptors, referred to as A_1, A_{2A}, A_{2B}, and A_3. The adenosine A_{2A} receptor ($A_{2A}R$) subtype is expressed predominantly in the basal ganglia of the central nervous system (CNS).[1] The $A_{2A}R$ plays an important role in modulating dopamine and glutamate neurotransmission, and regulating neuroinflammation.[2–6] Therefore, $A_{2A}R$ is generally associated with neurological and psychiatric disorders related to neuroinflammation and/or disturbed dopamine/glutamate signaling pathways, such as Huntington's disease (HD), Alzheimer's disease (AD), depression, schizophrenia, and Parkinson's disease (PD).[7,8]

Although little is known mechanistically about the role of $A_{2A}R$ in brain disorders so far, it is clear that the receptor is important in CNS functioning via its effects on neurons, glial cells, and vasculature.[9] This makes $A_{2A}R$ a potential therapeutic target, for example, in AD, HD, schizophrenia, and PD.[10–13] In addition,

Department of Nuclear Medicine and Molecular Imaging, University of Groningen, University Medical Center Groningen, Groningen, The Netherlands

Corresponding author:
Erik FJ de Vries, Department of Nuclear Medicine and Molecular Imaging, University of Groningen, University Medical Center Groningen, Hanzeplein 1, 9713GZ Groningen, The Netherlands.
Email: e.f.j.de.vries@umcg.nl

$A_{2A}R$ may act as a diagnostic biomarker in, for instance, HD and PD,[14–17] which could allow monitoring of disease progression.

Positron emission tomography (PET) with a suitable $A_{2A}R$ radioligand can be used to exploit the potential of $A_{2A}R$ as a biomarker by measuring its distribution and density. Furthermore, PET may also be a suitable technique to monitor changes in $A_{2A}R$ expression in the brain during the course of the disease, or to assess $A_{2A}R$ occupancy after administration of an (investigational) drug. The latter could be important for drug development, e.g. for establishing the optimal dosing regimen. [18F]MNI-444, [11C]TMSX, [11C]KW-6002, and [11C]SCH442416 are $A_{2A}R$ PET ligands that have been studied in human subjects.[16–22] [18F]MNI-444 displayed best properties among these tracers, with binding potential (BP_{ND}) values ranging from 2.6 to 4.9 in $A_{2A}R$-rich regions, and an average test–retest variability (TRV) of less than 10%.[18] Other tracers are hardly useful for $A_{2A}R$ quantification, because of the disadvantages such as low BP_{ND} in striatum, high extra-striatal binding and low target-to-non-target ratios.[16,17,19–22]

We have recently developed [11C]preladenant, the C-11 labeled analog of the drug preladenant. The in vivo assessment of this tracer in rats showed a better contrast in the PET images (i.e. larger striatum-to-cerebellum ratio) than published for other $A_{2A}R$ radioligands in rat studies.[23–27] The results suggest a great potential of [11C]preladenant to image $A_{2A}R$ in the brain. Another advantage of [11C]preladenant is that the toxicological profile of preladenant in humans is already known from clinical phase I/II/III studies, in which preladenant was investigated as a drug.[28] Therefore, expensive toxicity studies are not required anymore and the costs and timeline of tracer development can be reduced.

To determine the suitability of [11C]preladenant PET for $A_{2A}R$ quantification, we further evaluated the tracer by assessing pharmacokinetic modeling, test–retest reproducibility, and the feasibility of measuring $A_{2A}R$ occupancy in the rat brain.

Materials and methods

(E)-1,3-diethyl-8-(3,4-dimethoxystyryl)-7-methyl-3,7-dhydro-1H-purine-2,6-dione (KW-6002) was purchased from Axon Medchem BV (Groningen, The Netherlands).

Radiosynthesis

[11C]Preladenant was prepared according to the method described by Zhou et al.[27] The specific activity of [11C]preladenant was 81 ± 33 GBq/μmol (n = 26), and the radiochemical purity was always greater than 98%.

The tracer was formulated in ~15% ethanol in phosphate buffered saline as final product.

Animals

Adult male Wistar rats (n = 37, Hsd/Cpb:WU, 9–11 weeks age, 300–400 g, Harlan, The Netherlands) were housed in groups at a 12 h light/12 h dark circle and were fed with standard laboratory chow (RMH-B, The Netherlands) and water ad libitum. After arrival from the supplier, rats were acclimatized for at least 7 days. All experiments were approved by the Institutional Animal Care and Use Committee of the University of Groningen (DEC 6689B and DEC 6689G) and conducted in accordance with the Law on Animal Experiments of The Netherlands. All the animal study data were reported according to ARRIVE guidelines (Animal Research: Reporting In Vivo Experiment).

Brain metabolite analysis

The animals were sacrificed by extirpation of the heart at 60-min post injection. The brain was extracted and half of the brain (sagittal section) was homogenized with 1 mL of acetonitrile and then centrifuged at 3000 g for 3 min. The supernatant was filtered through a 0.45 μm Durapore (PVDF) filter (Millipore, Billerica, MA, USA). Samples (100 μL) were subsequently injected to a ultra-high performance liquid chromatography (UPLC) using an Acquity UPLC HSS T3 UHPLC column (1.8 μm, 3.0×50 mm^2) at a column temperature of 40°C and a gradient containing water (pH = 2 with $HClO_4$) and acetonitrile as mobile phase with flow rate of 1.1 mL/ min. The eluted fractions were collected every 30 s and measured with an automated well-counter (Compugamma 1282 CS, LKB-Wallac, Turku, Finland). The percentage of radioactive metabolites in the brain tissue was calculated as 100% − (total activity of intact tracer − activity of intact tracer in blood at 60-min post injection $\times$ 5%)/(total activity − total activity in blood at 60-min post injection $\times$ 5%) $\times$ 100%.

PET imaging

Prior to PET imaging, animals were anesthetized with isoflurane in medical air (5% isoflurane for induction, 1.0–2.5% isoflurane for maintenance) and kept on electronic heating pads during the study to avoid hypothermia. Cannulas were placed in a femoral vein for tracer injection and in a femoral artery for blood sampling. Six rats were i.p. injected with vehicle (50% dimethylacetamide (DMA) in saline) and six rats were i.p. injected with KW-6002 (1 mg/kg) in a 1 mg/mL solution of 50% DMA in saline 7–10 min prior to tracer injection. PET images were acquired using a Focus220

MicroPET scanner (Preclinical solutions, Siemens Healthcare Molecular Imaging, USA Inc.). Two rats were scanned simultaneously. The brains of both rats were positioned close to the center of the field of view. A transmission scan with a ^{57}Co point source was made for attenuation correction. Rats were i.v. injected with 66 ± 23 MBq (2.1 ± 1.7 nmol) [^{11}C]preladenant at a speed of 1 mL/min with an infusion pump for 1 min, and a 60-min dynamic PET scan was started. The injected mass was estimated to occupy $1.6 \pm 1.2\%$ A_{2A}Rs in rat striatum at the maximum uptake, being a standardized uptake value (SUV) of 2.2, and an A_{2A}R density of 953 fmol/mg protein.[29] Blood samples (each sample of 0.10–0.13 mL, 1.5–1.8 mL in total) were drawn from the femoral artery at 10, 20, 30, 40, 50, 60, 90 s and 2, 3, 5, 7.5, 10, 15, 30, 60 min after tracer administration. In all, 0.10–0.13 mL saline with 1% heparin was infused into the artery after each sampling to compensate for the blood loss. Radioactivity in 25 μL whole blood and 25 μL plasma (acquired by centrifugation of blood samples for 5 min at 1000 g) were measured with an automated well-counter and used as an arterial input function (with metabolite correction). List mode acquisition data was divided in 21 frames (6×10, 4×30, 2×60, 1×120, 1×180, 4×300, and 3×600 s). The data were reconstructed per time frame using an attenuation-weighted 2-dimensional ordered-subset expectation maximization algorithm (AW-OSEM2D). The 95 sagittal slices with a slice thickness of 0.8 mm were separated into one image for both rats with a 128×128 matrix and a pixel size of 0.47×0.47 mm^2. Datasets were fully corrected for random coincidences, decay, scatter, and attenuation.

PET data analysis

Summed PET images were manually aligned to a T2 magnetic resonance imaging (MRI) template of a rat brain with predefined volumes of interest (VOIs) for whole brain, total cortex, frontal cortex, occipital cortex, parietal cortex, striatum, midbrain, thalamus, hippocampus, and cerebellum. Time-activity curves (TACs, expressed as Bq/cc) for different VOIs were generated using Inveon Research Workplace software (Siemens Medical Solutions, Knoxville, TN), and were normalized to body weight (g) and injected dose (Bq) to obtain dynamic SUVs.

Tracer kinetic modeling

TAC data were analyzed using PMOD software (version 3.5, PMOD Technologies, Zürich, Switzerland). A mono-exponential function was fitted to a population-based intact tracer fraction obtained from our previous study.[27] The blood volume in the brain was fixed to 5%,

as the volume did not significantly affect distribution volume (V_T) estimation, being ~1% difference between 5% (ref. 30,31) and 3.6% (ref. 32) fits, and ~4% difference between 5% and 0% fits, whereas 5% blood volume fit gave smaller Akaike Information Criterion (AIC) values compared with 3.6% or 0% blood volume fits. A standard two-parameter (K_1, k_2) one-tissue compartment model (1TCM) and a four-parameter (K_1, K_1/k_2, k_3, k_4) two-tissue compartment model (2TCM), both with a metabolite corrected plasma input function, were used to fit the TACs. The best fitting model was selected based on AIC values. The V_T was obtained by modeling with the 2TCM and the Logan graphic analysis with t^* set to 10 min. Several reference tissue-based models, including simplified reference tissue model (SRTM), Ichise's multilinear reference tissue model (MRTM) with t^* set to 1 min, Ichise's multilinear reference tissue model 2 (MRTM2) with t^* set to 1 min, and the reference tissue Logan plot (RLogan) with t^* set to 5 min were used to estimate the BP_{ND} in striatum. The t^* was selected based on the goodness of fit, resulting V_T or BP_{ND} value (larger is better), and coefficient of variation (COV) of V_T or BP_{ND} (smaller is better). Cerebellum, midbrain, hippocampus, and occipital cortex were tested as reference regions. BP_{ND} obtained from the reference tissue-based models were compared with BP_{ND} obtained from k_3/k_4 (direct method) and calculated from the V_T determined with the 2TCM and the Logan plot using the formula $BP_{ND} = (V_T - V_{ND})/V_{ND}$ (ref. 33). The best reference regions were selected based upon the test–retest reliability, the BP_{ND} value in striatum, and between-subject variability of BP_{ND}.

Test–retest

To estimate test–retest reliability, five rats underwent two PET scans on consecutive days. The PET scans were performed as described above but without cannulation, blood sampling and KW-6002 or vehicle pretreatment. BP_{ND} in striatum was determined using SRTM, RLogan, MRTM, MRTM2, and SUV ratio (SUV_r) $-$ 1, using different reference regions. The SUV was the average SUV value from 25 till 60-min post injection. TRV was defined as

$$TRV = 2 \times \left| BP_{ND,test} - BP_{ND,retest} \right| / (BP_{ND,test} + BP_{ND,retest})$$

The test–retest reliability was quantified using intraclass correlation coefficient (ICC) with a one-way random effects model ICC (1, 1) (ref. 34):

$$ICC(1,1) = (BMS - WMS)/[BMS + (k-1)WMS],$$

where BMS is the mean sum of squares between subjects, WMS is the mean sum of squares within subjects, and k is the number of measurements, being 2 for test–retest. ICC was measured on a scale ranging from -1 to 1. One represents perfect reliability, whereas -1 indicates no reliability. An ICC ≥ 0.75 is considered as a good reliability.[35] The ICC was computed using **R** (http://www.r-project.org/).

$A_{2A}R$ occupancy

Eight baseline PET scans and 12 scans after administration of the selective $A_{2A}R$ antagonist KW-6002 were performed as described above but now without cannulation and blood sampling. The emission scan was extended to 90 min. The dose of KW-6002 (0.01, 0.03 (in duplicate), 0.04, 0.05, 0.06, 0.1 (in duplicate), 0.15, 0.3, 0.5, or 1 mg/kg) in a solution of 50% DMA in saline was i.p. administered 15–25 min before tracer injection. List mode acquisition data was divided in 23 frames (6×10, 4×30, 2×60, 1×120, 1×180, 4×300, 3×600, and 2×900 s). Receptor occupancy was calculated by the following equation:

$$Occupancy = \frac{BP_{ND,baseline} - BP_{ND,blocking}}{BP_{ND,baseline}} \times 100\%,$$

where BP_{ND} was derived from SRTM, RLogan, SUV_r $- 1$, and modified SUV ratio ($mSUV_r$) $- 1$, using midbrain, cerebellum, or occipital cortex as the reference region. The modification factors for $mSUV_r - 1$ were determined by Deming linear regression between SUV_r $- 1$ and SRTM or RLogan derived BP_{ND}. The occupancy (%) was plotted against the drug dose and the dose-occupancy curve was fitted in GraphPad Prism (version 5.01, GraphPad Software, Inc.) with a one site-specific binding model using the following formula:

$$Occupancy(\%) = 100 \times Occ_{max} \times D^{hillslope}$$
$$/(D^{hillslope} + ED_{50}^{hillslope}),$$

where Occ_{max} is the maximum occupancy, ED_{50} is the drug dose which corresponds to 50% occupancy, and D is the drug dose. The striatal BP_{ND} and ED_{50} were estimated from the 90-min acquisition as well as from the first 60 min of this acquisition. The values from both estimates were compared.

Statistics

All results are expressed as mean $\pm$ standard deviation (SD). Unpaired two-tailed t-test with Bonferroni correction for multiple comparisons was used to assess the difference in plasma activity between vehicle and KW-6002 pretreatment groups. Paired two-tailed t-test with Bonferroni correction for multiple comparisons was used to assess the difference between BP_{ND} and $(m)SUV_r - 1$, the difference in BP_{ND} between direct method and indirect methods, and the difference in COV between 60- and 90-min acquisitions. Two-way ANOVA with Bonferroni post-tests was used to evaluate the effects of KW-6002 pretreatment and VOIs on V_T and BP_{ND}. Repeated measures two-way ANOVA with Bonferroni post-tests was used to assess the difference in AIC, V_T, and BP_{ND} between models and VOIs, the difference in BP_{ND} between test–retest and VOIs/models, and the difference in BP_{ND} between acquisition times and VOIs. Bland–Altman plot (difference (Δ) vs. mean) and one sample t-test were used to judge the bias (Δ) in BP_{ND} obtained from Logan plot and reference tissue-based modeling methods as compared with BP_{ND} calculated from 2TCM. Δ (%) was computed as

$$\Delta = 2 \times 100 \times (BP_{ND,1} - BP_{ND,2})/(BP_{ND,1} + BP_{ND,2}),$$

where $BP_{ND,1}$ was derived from 2TCM, Logan plot, SRTM, MRTM, and RLogan, and $BP_{ND,2}$ was always calculated from 2TCM. Deming linear regression was used to compare acquisition durations, and $SUV_r - 1$ and BP_{ND}. A probability value (p) < 0.05 was considered statistically significant.

Results

Plasma clearance and brain metabolism of [¹¹C]preladenant

Figure 1(a) shows the plasma clearance of the tracer during the 60-min scan. KW-6002 pretreatment did not significantly affect the tracer kinetics in plasma. The plasma curves were corrected with a mono-exponential fitted population-based intact-tracer function. The metabolite corrected plasma curve at baseline was well described with a two-phase exponential function, with a $t_{1/2}\alpha$ of 0.59 ± 0.37 min, and $t_{1/2}\beta$ of 22.24 ± 4.68 min (n = 6). At 60-min post tracer injection, $17 \pm 5\%$ (n = 3) of the total activity in the brain tissue was due to the radioactive metabolites.

Tracer kinetic modeling

The tracer kinetics in rat brain is better described with a 2TCM with a fixed blood volume of 5% than a 1TCM with a fixed blood volume of 5% (Figure 1(b) and (c)). The 2TCM fits showed significantly (p < 0.001) lower AIC values compared with 1TCM fits (Bonferroni post-tests), whereas no difference in average AIC values was observed between brain regions, and there was no interaction between model and VOI (repeated measures
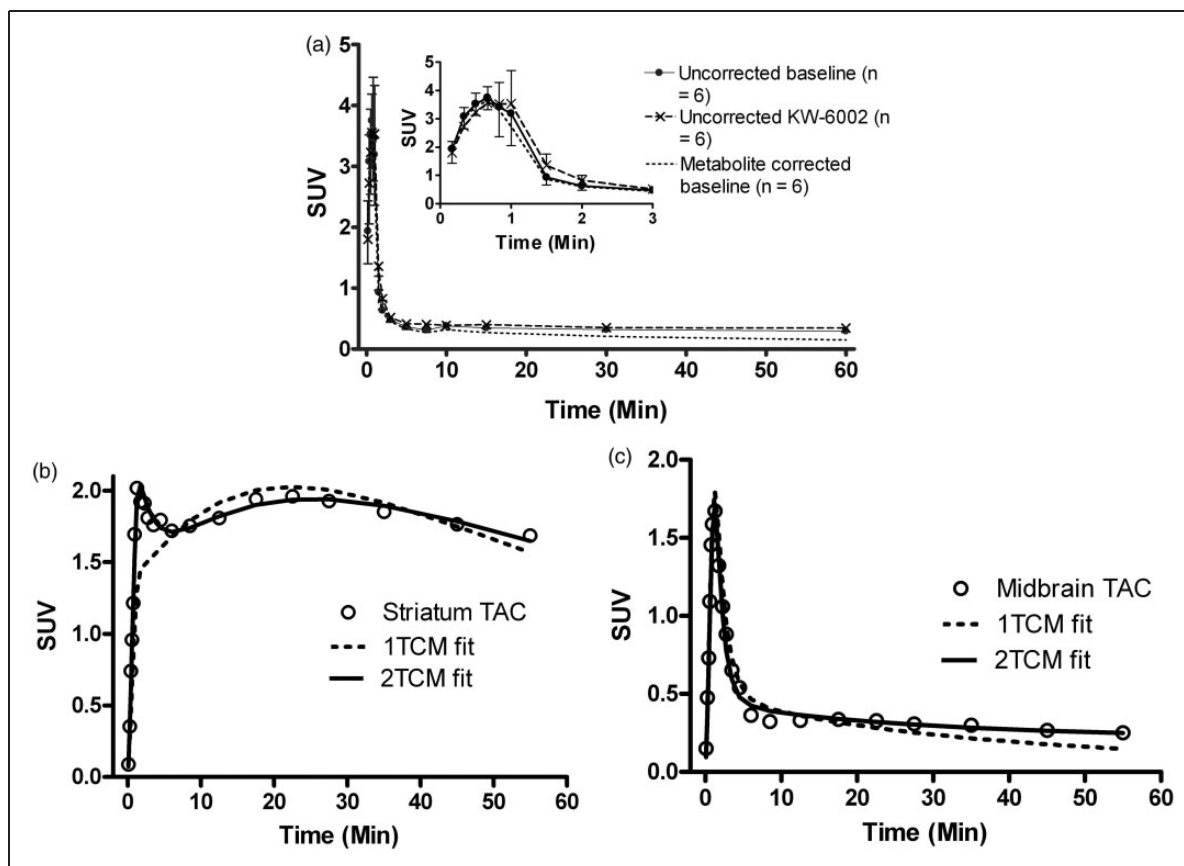
Figure 1. (a) Kinetics of $[^{11}C]$preladenant in rat plasma. The insert shows the first 3 min of the plasma kinetics. Error bars indicate standard deviation. (b, c) Representative TACs and modeling fits of individual brain regions at baseline. (b) TAC of striatum with 1TCM and 2TCM fits with a fixed blood volume of 5%. (c) TAC of midbrain with 1TCM and 2TCM fits with a fixed blood volume of 5%. TACs: time-activity curves; 1TCM: one-tissue compartment model; 2TCM: two-tissue compartment model.

Table 1. V_T (mean $\pm$ SD) obtained from 2TCM and Logan plot ($n = 6$).

Brain region	2TCM-baseline	2TCM-blocking	Logan-baseline	Logan-blocking
Striatum	10.50 ± 1.91	2.04 ± 0.38***	9.88 ± 1.74	2.00 ± 0.36***
Midbrain	1.47 ± 0.17	1.51 ± 0.18	1.47 ± 0.13	1.38 ± 0.15
Hippocampus	1.58 ± 0.22	1.52 ± 0.30	1.48 ± 0.17	1.35 ± 0.10
Cerebellum	1.58 ± 0.14	1.41 ± 0.27	1.57 ± 0.10	1.40 ± 0.23
Occipital cortex	1.55 ± 0.15	1.46 ± 0.16	1.50 ± 0.10	1.45 ± 0.14

Significant differences against baseline are indicated by ***$p < 0.001$. SD: standard deviation; 2TCM: two-tissue compartment model.

two-way ANOVA). For the striatal TAC (Figure 1(b)), the 2TCM fitted the data much better than the 1TCM, particularly for the first 10 min. In the extra-striatal regions, 1TCM failed to describe the later time points of TACs (Figure 1(c)).

V_T was estimated by 2TCM and Logan graphic analysis (Table 1). The effects of model and brain region on V_T at baseline were analyzed. There was a strong interaction between model and brain region ($p < 0.001$), and both model and VOI significantly ($p < 0.001$) affected average V_T (repeated measures two-way ANOVA). Striatal V_T determined by the 2TCM was 10.5 ± 1.9, which was slightly (5.8%) but significantly ($p < 0.001$) higher compared with V_T estimation by Logan plot (9.9 ± 1.7). Both models provided comparable V_T values of ~ 1.5 in extra-striatal

regions (Bonferroni post-tests). KW-6002 pretreatment significantly (p < 0.001) reduced the V_T in striatum to ~2.0, whereas no significant difference was found between vehicle and KW-6002 pretreatment in other brain regions (two-way ANOVA with Bonferroni post-tests). The V_T data of parietal cortex, frontal cortex, thalamus, cortex total, and whole brain are listed in Supplementary Table 1 and are not discussed here, because these brain regions are affected by spill-over from striatum and harderian glands with high tracer uptake. Several reference regions, including midbrain, hippocampus, cerebellum, and occipital cortex were selected and tested in reference region models to predict BP_{ND}. These selected regions are relatively large brain structures lacking $A_{2A}R$ specific binding sites.[36] Furthermore, they are away from striatum and harderian glands, so that the spill-over effect is avoided. Therefore, the V_T values obtained from these regions were smaller and more stable than the values of other extra-striatal regions ($V_T = $ ~1.5 vs. $V_T = $ ~1.5–2.5, COV = 6–14% vs. COV = 8–20%) and were not affected by the KW-6002 pretreatment (Table 1 and Supplementary Table 1). Such properties make them the suitable candidates as reference regions to calculate striatal BP_{ND}.

BP_{ND} values estimated by k_3/k_4 (direct method) are shown in Supplementary Table 2. The BP_{ND} values were significantly (p < 0.001) different among brain regions for vehicle/KW-6002 treatment. Both treatment and VOI strongly (p < 0.001) affected average BP_{ND} (two-way ANOVA). Striatal BP_{ND} in vehicle treated animals was 9.17 ± 1.90, the value was significantly (p < 0.001) reduced to ~1.38 ± 0.63 with KW-6002 pretreatment, whereas the pretreatment did not alter the BP_{ND} in reference regions (Bonferroni post-tests). Striatal BP_{ND} at baseline was also obtained by indirect methods using a reference region (Supplementary Table 3). Indirect methods estimated similar BP_{ND} values of 5.0–6.1, which were ~40% smaller than BP_{ND} calculate from the direct method. However, the between-subject variability with indirect methods (8–19% COV) was smaller than the variability of the direct method (20% COV). Indirect methods with midbrain or hippocampus as the reference tissue seemed to produce less variable results (~10% COV), compared with other reference regions (~17% COV) (Supplementary Table 3 and Figure 2). Midbrain as the reference region estimated significantly (p < 0.05) higher BP_{ND} values in striatum, regardless of the model used (repeated measures two-way ANOVA with Bonferroni post-tests). We compared various reference regions for the striatal BP_{ND} values at baseline obtained from Logan plot and reference tissue-based modeling methods with the BP_{ND} calculated from 2TCM as the gold standard. Relative to the 2TCM, a significantly (p < 0.05)

negative bias (Δ) (up to 13.2%) was found with Logan plot and reference tissue-based methods for all reference regions in most cases (one-sample t-test) (Figure 2 and Supplementary Table 4). Such bias was also demonstrated by the linear regression of the striatal BP_{ND} values obtained from SRTM and RLogan against BP_{ND} values calculated from 2TCM, showing slopes of 0.91 for RLogan and 0.87 for SRTM when the midbrain was used as the reference region (Supplementary Figure 1).

SRTM and MRTM estimated comparable k_2' values (Supplementary Table 5). The variability was slightly smaller with SRTM than MRTM. Therefore, k_2' values determined by SRTM ($0.39 \pm 0.06 - 0.45 \pm 0.02 \, \text{min}^{-1}$) were used in RLogan and MRTM2.

Test–retest

Test and retest BP_{ND} values for SRTM, RLogan, and $SUV_r - 1$ are presented in Table 2. TRV and ICC for all methods are listed in Supplementary Table 6. The average retest BP_{ND} values were significantly (p < 0.01) smaller than the test results, and such difference was comparable between VOIs or models, whereas differences in VOI or model did not significantly affect average BP_{ND} (repeated measures two-way ANOVA), nor the test and retest BP_{ND} values (Bonferroni post-tests). The average TRV was less than 10%, which was similar across VOIs and models. The ICC values were fairly homogenous for all VOIs and models, ranging from 0.83 to 0.94, except for models with hippocampus as the reference region, showing an ICC of 0.38–0.43. Because of lacking of test–retest reliability, hippocampus was no longer assessed in the occupancy study. Occipital cortex displayed the lowest within-subject variability (TRV = 4.6–6.4%) and highest test–retest reliability (ICC = 0.91–0.94) compared with other reference regions. Since MRTM and MRTM2 did not show better results compared with SRTM and RLogan in terms of resulting BP_{ND} value and the inter-/intra-subject variability of BP_{ND}, these bi-linear regression methods were not assessed in the occupancy study.

$A_{2A}R$ occupancy

Pretreatment of KW-6002 at 15–25 min before administration of [^{11}C]preladenant decreased the tracer uptake in striatum in a dose-dependent manner (Figure 3). BP_{ND} in striatum was determined by SRTM, RLogan, and (m)$SUV_r - 1$ with a static scan duration of 35 min, starting at 25-min post injection, using midbrain, cerebellum, or occipital cortex as the reference region. The correlation between striatal BP_{ND} obtained from 90-min acquisition and from 60-min
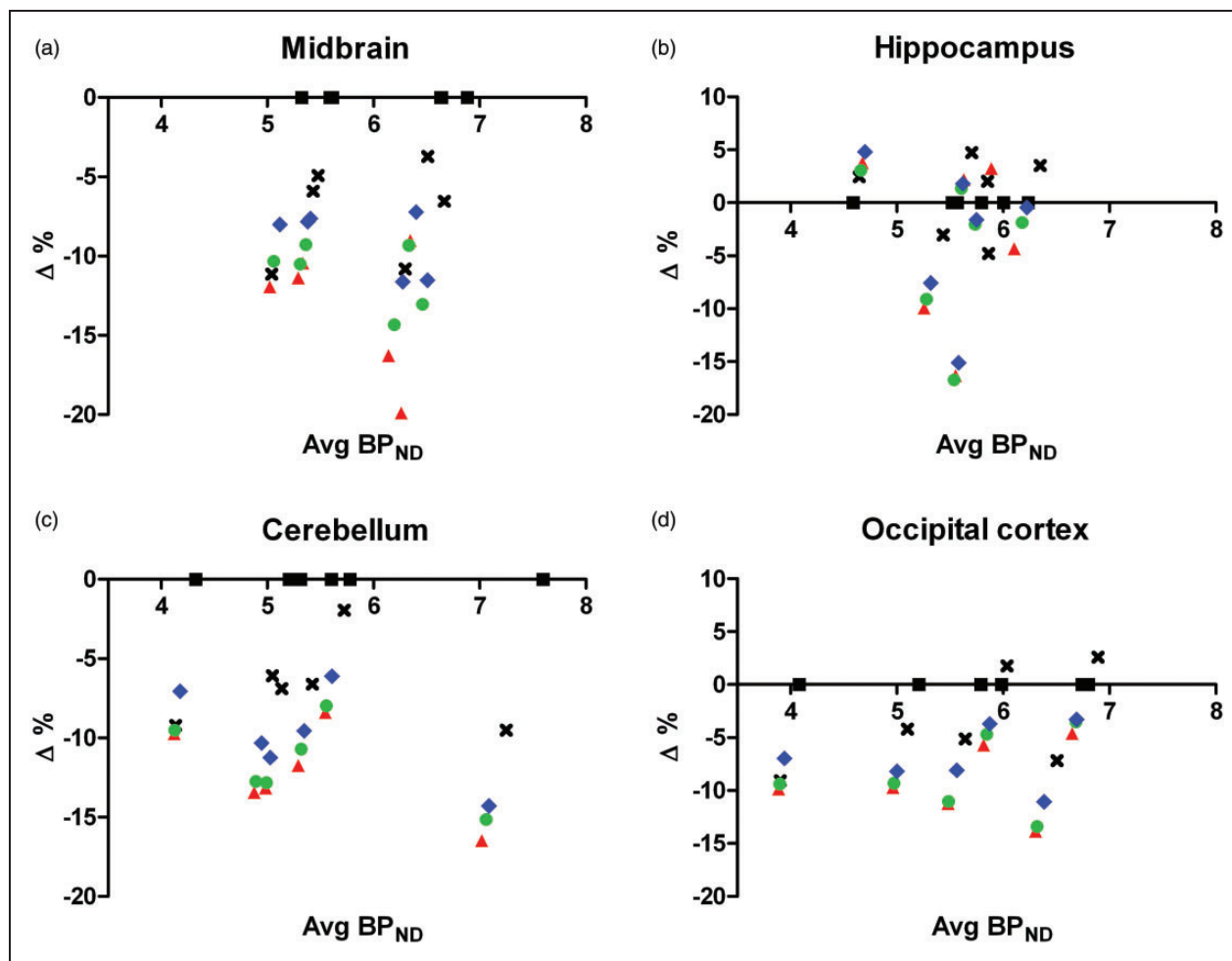
Figure 2. Bland–Altman plot for midbrain (a), hippocampus (b), cerebellum (c), and occipital cortex (d) with different modeling methods to obtain striatal BP_{ND}. $Avg\ BP_{ND} = (BP_{ND,1} + BP_{ND,2})/2$, $\Delta = 2 \times 100 \times (BP_{ND,1} - BP_{ND,2})/(BP_{ND,1} + BP_{ND,2})$, where $BP_{ND,1}$ was derived from 2TCM (black square), Logan plot (black cross), SRTM (red triangle), MRTM (green circle), and RLogan (blue diamond), and $BP_{ND,2}$ was always calculated from 2TCM. Each point represents the data of an individual animal (n = 6). BP_{ND} obtained from 2TCM and Logan plot was calculated from the V_T using the formula $BP_{ND} = (V_T - V_{ND})/V_{ND}$.
2TCM: two-tissue compartment model; SRTM: simplified reference tissue model; MRTM: multilinear reference tissue model; RLogan: reference tissue Logan plot.

Table 2. Test and retest striatal BP_{ND} (mean ± SD) values obtained from different models and reference regions (n = 5).

Reference region	SRTM		RLogan		[a]SUV_r −1	
	Test	Retest	Test	Retest	Test	Retest
Midbrain	5.81 ± 0.85	5.49 ± 0.94	5.96 ± 0.90	5.50 ± 1.04	6.37 ± 0.93	5.79 ± 1.10
Hippocampus	5.38 ± 0.38	5.02 ± 0.67	5.46 ± 0.39	5.10 ± 0.68	5.64 ± 0.42	5.34 ± 0.67
Cerebellum	5.72 ± 1.23	5.38 ± 1.15	5.87 ± 1.30	5.55 ± 1.16	6.37 ± 0.93	5.94 ± 1.40
Occipital cortex	5.69 ± 1.01	5.39 ± 0.89	5.79 ± 1.09	5.44 ± 0.94	6.05 ± 1.22	5.68 ± 1.24

[a]$SUV_r = SUV_{striatum}/SUV_{reference}$. SD: standard deviation; SRTM: simplified reference tissue model; RLogan: reference tissue Logan plot.

acquisition was studied using Deming linear regression. The BP_{ND} values at 60 min were plotted against BP_{ND} values at 90 min (Figure 4(a) and (b)). Both SRTM and RLogan showed a strong correlation between

acquisition times, with slopes close to 1 (1.00–1.03) and a very small y-intercept of around 0.06. In comparison with the 60-min acquisition, the 90-min acquisition estimated marginally smaller (1.8–3.6%) BP_{ND}
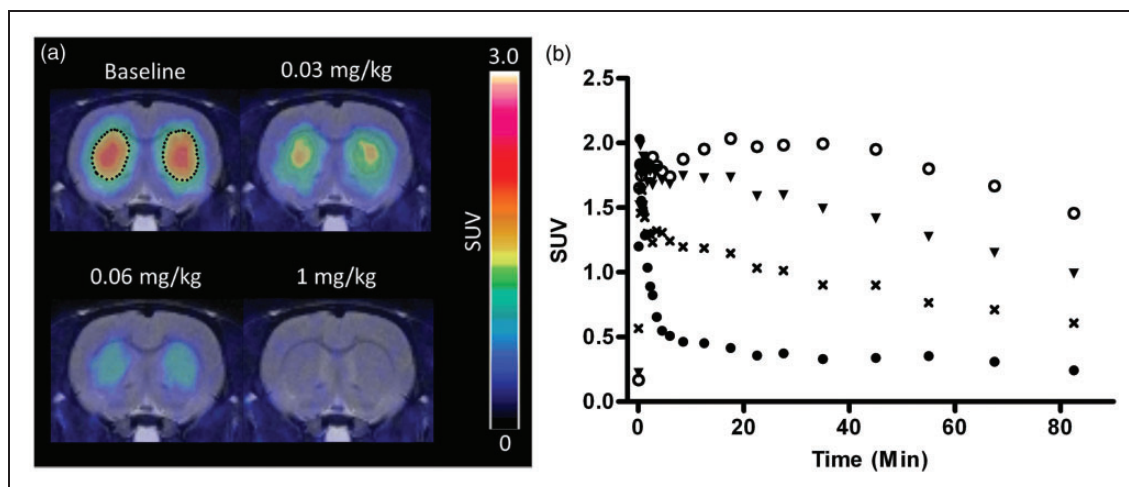
Figure 3. Representative PET images of the coronal view of the rat brain (summed from 30 to 90 min) (a) and corresponding TACs in striatum (b) at baseline (open circle) and after i.p. injection of KW-6002 at 0.03 (triangle), 0.06 (cross), and 1 (closed circle) mg/kg (occupancy of 37%, 67%, and 98%, respectively). The PET images were merged onto the MRI template. Striatum at baseline were outlined by dots.
PET: positron emission tomography; TACs: time-activity curves; MRI: magnetic resonance imaging.

values at baseline. Deming linear regression was also used to assess the correlation between $SUV_r - 1$ and BP_{ND} derived from pharmacokinetic modeling for 60-min acquisition (Figure 4(c) and (d)). A high agreement was found between these methods, indicating that $SUV_r - 1$ is also a robust parameter to predict BP_{ND}. The striatal BP_{ND} can be calculated from $SUV_r - 1$ corrected by the following equation:

$$BP_{ND} = mSUV_r - 1 = [(SUV_r - 1) - y\,intercept]/slope,$$

where the y-intercept and slope were obtained from Deming linear regression (Figure 4(c) and (d)).

To estimate the ED_{50} of KW-6002, the dose-occupancy curve was fitted with the equation:

$$Occupancy(\%) = 100 \times Occ_{max} \times D^{hillslope}$$
$$/(D^{hillslope} + ED_{50}^{hillslope})$$

The hillslope was calculated to be approximately 1, indicating the binding pattern of monomer one-site binding. Then the hillslope value was fixed to 1 for all calculations. Occ_{max} (maximum occupancy) was estimated to be ~87–103% with a standard error of ~4–6%, and a 95% confidence interval of 73–123% for the tested reference regions and models. $A_{2A}R$ occupancy as well as ED_{50} estimates were similar between models and scan durations with the same reference regions (<10% difference between models and <5% difference between acquisition times) (Figure 5). However, larger differences in ED_{50} estimation were observed between

reference regions: KW-6002 ED_{50} estimates for i.p. injection were 0.056 ± 0.003, 0.062 ± 0.002, and 0.044 ± 0.002 mg/kg for midbrain, cerebellum, and occipital cortex as the reference region, respectively.

Discussion

This study demonstrates that [^{11}C]preladenant is a suitable PET tracer for the quantification of available $A_{2A}R$ binding sites in the rat brain. The tracer displayed high uptake in striatum and low and homogenous uptake in all extra-striatal regions. The regional distribution of [^{11}C]preladenant is in agreement with the known $A_{2A}R$ expression in the rat brain,[36] as the receptors are predominantly expressed in striatum only. An $A_{2A}R$ subtype selective antagonist, KW-6002 (K_i value: $A_{2A}R = 2.2$ nM, $A_1R = 150$ nM (ref. 37)) significantly reduced the tracer uptake in striatum by 80%. However, the V_T in striatum was till 40% higher than the values in the reference brain regions (Table 1). A complete blockade could be achieved with higher doses of KW-6002. However, 1 mg/kg was the highest dose without adverse effects. Test–retest results indicate that [^{11}C]preladenant PET is highly reproducible for the imaging of $A_{2A}Rs$. The $A_{2A}R$ occupancy study reveals that the tracer uptake is sensitive to the changes in available $A_{2A}Rs$. The sufficiently large dynamic range ($BP_{ND} \approx 5.5$ at baseline and < 0.5 with complete blockade, Supplementary Table 3) allows [^{11}C]preladenant to estimate $A_{2A}R$ occupancy in striatum by KW-6002 as well as other $A_{2A}R$-targeting molecules with high accuracy. Thus, [^{11}C]preladenant
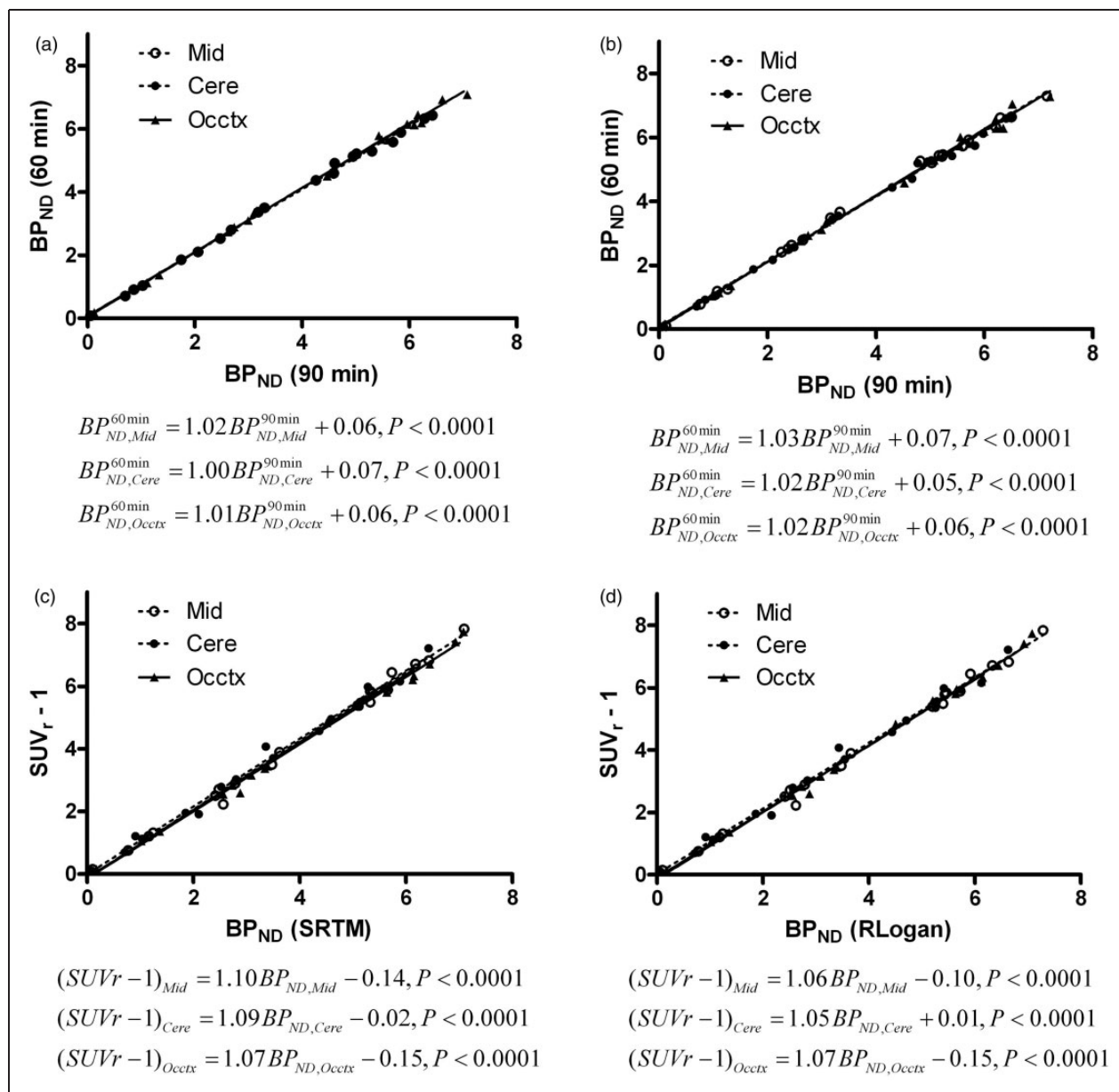
Figure 4. Correlation of striatal BP_{ND} obtained from 60-min acquisition with BP_{ND} obtained from 90-min acquisition (a, b), and correlation of $SUV_r - 1$ with BP_{ND} obtained from 60-min acquisition (c, d). (a, c) BP_{ND} was predicted by SRTM; (b, d) BP_{ND} was predicted by RLogan. $SUV_r = SUV_{striatum}/SUV_{reference}$.
Mid: midbrain, Cere: cerebellum, Occtx: occipital cortex; SRTM: simplified reference tissue model; RLogan: reference tissue Logan plot.

is a good tool to aid the development of $A_{2A}R$ drugs if confirmed in humans.

Several plasma input-dependent (2TCM and Logan plot) and reference tissue-based (SRTM, MRTM, MRTM2, and RLogan) modeling methods as well as (m)$SUV_r - 1$ were applied to calculate V_T and/or BP_{ND}. Regarding the BP_{ND} estimation, four reference regions have been tested with indirect models. There are two purposes to test different reference regions: (a) to find proper reference regions with negligible receptor expression, which are able to estimate target BP_{ND}

with high value, low standard error, and a high test–retest reproducibility; and (b) to have suitable alternative reference regions. Because $A_{2A}Rs$ are also expressed in glial cells that are involved in regulating neuroinflammation, $A_{2A}R$ tracers could also be used to study $A_{2A}R$ changes in animal models with neuroinflammation, for example, the herpes simplex virus infected rat model. In this case, midbrain and cerebellum are not proper reference regions anymore, because these regions are affected by the virus and associated with an increased level of $A_{2A}R$. Then, we may choose
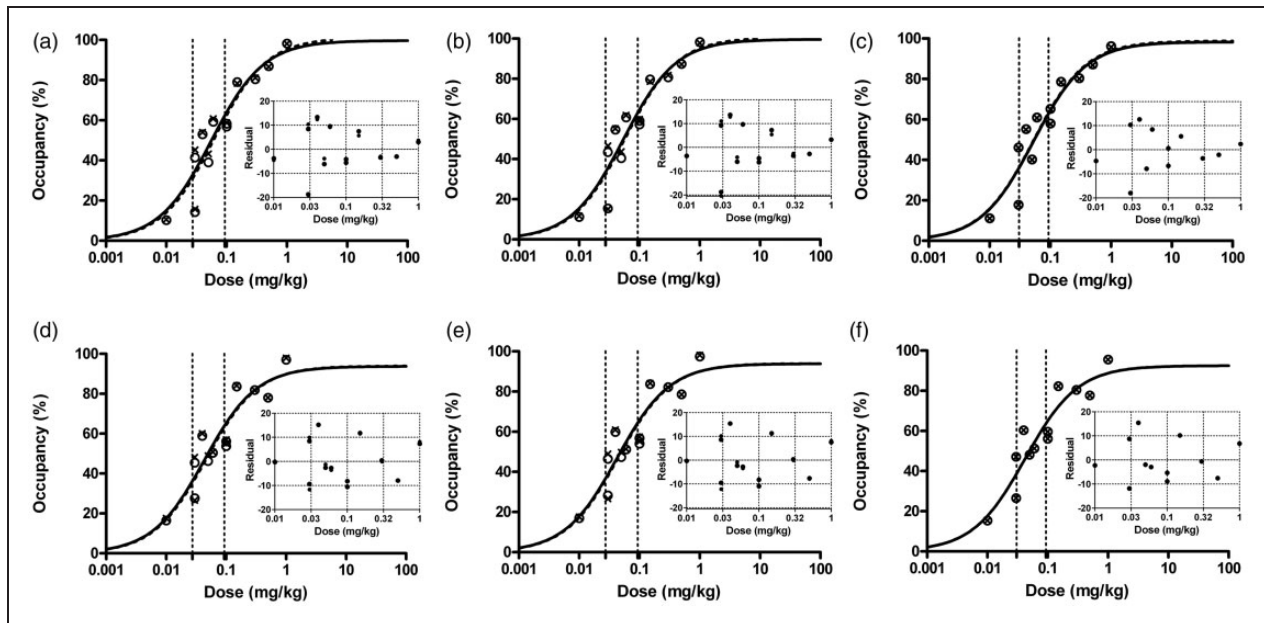
Figure 5. Striatal $A_{2A}R$ occupancy against KW-6002 doses. (a–c) Occupancy was determined by SRTM (a), RLogan (b), and $mSUV_r -$ 1 (c), using midbrain as the reference region. (d–f) Occupancy was determined by SRTM (d), RLogan (e), and $mSUV_r -$ 1 (f), using occipital cortex as the reference region. (a, b, d, e) Circle: occupancy for 60-min acquisition; Cross: occupancy for 90-min acquisition; Curved dotted line: 60-min acquisition fit; Solid line: 90-min acquisition fit. (c, f) Circle: occupancy for $mSUV_r -$ 1, based on RLogan correction; Cross: occupancy for $mSUV_r -$ 1, based on SRTM correction; Curved dotted line: RLogan corrected $mSUV_r -$ 1 fit, Solid line: SRTM corrected $mSUV_r -$ 1 fit. The areas between vertical dotted lines represent 95% confidence interval of ED_{50}. The inserts indicate residuals of regression. Correction factors for $mSUV_r -$ 1 were determined by Deming linear regression between $SUV_r -$ 1 and SRTM or RLogan derived BP_{ND}.

$A_{2A}R$: A_{2A} receptor; SRTM: simplified reference tissue model; RLogan: reference tissue Logan plot.

a less infected region (occipital cortex) as the reference region instead.

V_T and BP_{ND} predictions with all models and reference regions were in agreement with each other, except for the striatal BP_{ND} estimation with the direct method, which was about 60% larger than the BP_{ND} estimated by indirect methods. Indirect methods might have underestimated BP_{ND} because of (a) the presence of radioactive metabolites in the brain, which contributed $\sim$17% of the total activity in the brain at 60-min post injection. The brain metabolites reduced the target-to-background ratio, leading to an underestimation in BP_{ND} when the indirect methods were applied. When the V_T values were corrected by subtracting the V_T contribution by 17% radioactive metabolites, the BP_{ND} calculated from $BP_{ND} = (V_T - V_{ND})/V_{ND}$ became $\sim$8.9, which was comparable with k_3/k_4 of 9.2. Also because of the radioactive metabolites in the brain, when the 2TCM was used to fit tracer TACs, a specific distribution volume of 0.6–1.1 was found in reference regions which was not affected by KW-6002 blockade. The presence of radioactive metabolites could also explain the difference between the direct method and indirect methods derived BP_{ND} in striatum

with KW-6002 pretreatment (Supplementary Tables 2 and 3). The brain metabolite could theoretically be a problem with this tracer. However, it didn't show much effect on the BP_{ND} stability, as only $\sim$3% difference was observed in BP_{ND} between 90-min and 60-min acquisition data; (b) noise-induced negative bias with graphical analysis.[38] For Ichise's multilinear regression, it was shown that a 5% average noise in the TAC can result in a 75% underestimation of BP_{ND} at a true BP_{ND} of 3 (ref. 39). Such underestimation is more pronounced at high noise level and high actual V_T and BP_{ND}; (c) Violations of assumptions with SRTM fit.[40] For example, the tracer kinetics could be fitted well with the 2TCM, but not with the 1TCM. Such violation resulted in an underestimation of BP_{ND}. On the other hand, the BP_{ND} calculated from the direct method might be biased due to the polar radioactive metabolites penetrating the blood-brain-barrier. Reference tissue-based BP_{ND} values displayed much lower variability ($\sim$10% COV) compared with the variability of k_3/k_4 and V_T ($\sim$18–20% COV) in striatum. This is a well-known aspect of reference tissue models and is related to the number of fit parameters. V_T seems to be more variable than BP_{ND}, probably due to the

variability in the plasma sample measurements. Therefore, we consider that BP_{ND} predicted from indirect methods is more robust than k_3/k_4 and V_T.

In addition, we compared the striatal BP_{ND} values predicted from different reference tissue models, using 2TCM as the gold standard. BP_{ND} estimated from reference tissue-based models correlated well ($R^2 > 0.99$) with 2TCM estimation (Supplementary Figure 1). However, a small (up to 13.2%) negative bias (Supplementary Table 4) was observed with reference tissue-based methods. Here, we consider that the accuracy in BP_{ND} prediction is less important than other properties like the robustness of model-parameter values and the model complexity. Therefore, BP_{ND} derived from reference tissue-based modeling methods was used to study the test–retest reproducibility of [^{11}C]preladenant PET and to characterize $A_{2A}R$ occupancy.

The test–retest experiment showed that the striatal BP_{ND} values for the retest were slightly lower (<10%) with ~10% larger between-subject variability compared with test values. The receptor occupancy by the PET tracer during the test scan was estimated to be ~2–7%, provided an $A_{2A}R$ density of 300–953 fmol/mg protein in striatum.[1,29,41] We assume that the occupancy decreased at least 60% after 24 h (ref. 42), then ~1–3% of the receptors were occupied by the cold tracer. However, this number cannot completely explain the underestimation of 4–9% with retest. Therefore, we consider that other factors such as anesthesia during the test scan may lead to the underestimation of BP_{ND} with retest.

In addition, we compared BP_{ND} and ED_{50} values obtained from the 90-min acquisition with the values obtained from the 60-min acquisition in the occupancy study. The BP_{ND} as well as ED_{50} predictions were very similar between models and acquisition times (Figures 4 and 5). The slightly (<3%) higher BP_{ND} values at baseline obtained from the 60-min acquisition could be explained by the slow accumulation of radioactive metabolites in the brain, leading to a reduced BP_{ND} value for 90-min acquisition. Furthermore, 60-min acquisition showed improved precision in BP_{ND} prediction, with significantly ($p < 0.05$) lower COV compared with COV of 90-min acquisition. Therefore, 60-min acquisition provides better estimation of BP_{ND} in rat brain, compared with 90-min acquisition.

The kinetic modeling and test–retest experiments showed that all reference tissue-based models, including SRTM, MRTM, MRTM2, and RLogan with different reference brain regions, including midbrain, cerebellum, and occipital cortex provided comparable results, with a high BP_{ND} value in striatum with small between-subject variability and high test–retest reliability. However, in comparison with midbrain and occipital cortex, cerebellum seems to be less favorable, with a slightly higher between-subject and TRV than the other two reference regions.

In the $A_{2A}R$ occupancy study, ~30% difference was found in ED_{50} prediction between modeling methods using occipital cortex as the reference region and models using midbrain or cerebellum as the reference region. It is difficult to determine which value is more reliable and which reference region is better than the rest in the $A_{2A}R$ occupancy study, since the 95% confidence interval for ED_{50} is quite wide for all methods, being around 0.02–0.09 mg/kg (Figure 5). Taking into account factors like the need of blood sampling, complexity of the model, intra- and inter-individual variability, and the value of BP_{ND} in striatum, we consider that SRTM with midbrain or occipital cortex as the reference tissue to be the preferable model for striatal $A_{2A}R$ quantification, as SRTM is simpler than RLogan and MRTM2, which require a priori k_2' estimation, and SRTM is slightly more robust than MRTM (Supplementary Table 6).

An interesting finding in this study is the suitability of SUV_r to predict striatal BP_{ND}, in terms of comparable COV and test–retest reliability between $SUV_r - 1$ and BP_{ND} (Table 2 and Supplementary Table 6), a strong correlation between the two parameters (Figure 4(c) and (d)), and the feasibility of (m)$SUV_r - 1$ to study $A_{2A}R$ occupancy (Figure 5(c) and (f)). In the occupancy study, both m$SUV_r - 1$ and $SUV_r - 1$ predicted comparable ED_{50} of KW-6002 with the value obtained from BP_{ND} with pharmacokinetic modeling, indicating that m$SUV_r - 1$ and $SUV_r - 1$ are robust parameters to predict BP_{ND} and study $A_{2A}R$ occupancy in striatum. Therefore, the PET acquisition procedure can be further reduced to a 35-min static scan, starting at 25-min post tracer injection. However, we should use (m)$SUV_r - 1$ with caution especially in pathological conditions. Since the regional perfusion might have changed under such conditions and thus might have different effects on SUV_r and BP_{ND}. The usefulness of (m)$SUV_r - 1$ for striatal $A_{2A}R$ quantification in other experimental setups needs to be further explored.

During the last two decades, many PET tracers have been developed for the imaging of $A_{2A}Rs$ in the brain. The most promising [^{18}F]MNI-444 was recently tested in the rhesus monkeys[42] and human subjects.[18] The tracer showed good brain penetration, high BP_{ND} values in $A_{2A}R$-rich regions and high test–retest reproducibility. However, slow kinetics might be the problem with this tracer. The tracer uptake peaked in $A_{2A}R$-rich regions at around 40- to 60-min post injection in the human and monkey brain. For the monkey study, a 120-min acquisition is required to quantify the tracer kinetics, with a 6–9% overestimation of striatal BP_{ND}

with 120-min acquisition compared with 180-min acquisition. For the human study, the 90-min acquisition overestimated striatal BP_{ND} by $\sim$9% as compared with 210-min acquisition. In our rat study, $[^{11}C]$preladenant showed faster kinetics, with the highest uptake in striatum at 22.5-min post injection. A 60-min acquisition is sufficient to estimate BP_{ND}, with marginally overestimation of BP_{ND} of <3% on average as compared with BP_{ND} values measured with 90-min acquisition. However, the direct comparisons between studies are difficult because of the different species and experimental setups in the studies.

Conclusions

This study shows that $[^{11}C]$preladenant selectively binds to A_{2A}Rs in the brain. The tracer has a favorable pharmacokinetic profile. The tracer displayed high BP_{ND} in striatum with excellent test–retest reproducibility and ability to assess the changes of available A_{2A}Rs in the brain. A 60-min acquisition protocol using the SRTM with midbrain or occipital cortex as the reference region for kinetic modeling is the preferred method to quantify A_{2A}Rs in the brain. The acquisition protocol can be further reduced to a 35-min static scan to estimate BP_{ND} with high accuracy since BP_{ND} and SUV_r are closely correlated. The results indicate that $[^{11}C]$preladenant is a very promising A_{2A}R tracer that warrants further validation in non-human primates and human subjects.

Declaration of conflicting interests

The author(s) declared no potential conflicts of interest with respect to the research, authorship, and/or publication of this article.

Authors' contributions

Xiaoyun Zhou, Rudi AJO Dierckx, Philip H Elsinga, and Erik FJ de Vries conceived and designed the experiment and were involved in interpretation of the data. Xiaoyun Zhou and Shivashankar Khanapur carried out the experiments. Xiaoyun Zhou, Johan R de Jong, and Antoon TM Willemsen analyzed and interpreted the experimental data. Xiaoyun Zhou drafted the manuscript. All authors corrected and improved the contents of the manuscript. All authors

agreed to publish the manuscript in the *Journal of Cerebral Blood Flow & Metabolism*.

References

1. Jarvis MF, Schulz R, Hutchison AJ, et al. [3H]CGS 21680, a selective A2 adenosine receptor agonist directly labels A2 receptors in rat brain. *J Pharmacol Exp Ther* 1989; 251: 888–893.
2. Ferré S, Quiroz C, Orru M, et al. Adenosine A(2A) receptors and A(2A) receptor heteromers as key players in striatal function. *Front Neuroanat* 2011; 5: 1–8.
3. Nishi A, Liu F, Matsuyama S, et al. Metabotropic mGlu5 receptors regulate adenosine A2A receptor signaling. *Proc Natl Acad Sci USA* 2003; 100: 1322–1327.
4. Schiffmann SN, Fisone G, Moresco R, et al. Adenosine A2A receptors and basal ganglia physiology. *Prog Neurobiol* 2007; 83: 277–292.
5. Haskó G, Pacher P, Vizi ES, et al. Adenosine receptor signaling in the brain immune system. *Trends Pharmacol Sci* 2005; 26: 511–516.
6. Rebola N, Simões AP, Canas PM, et al. Adenosine A2A receptors control neuroinflammation and consequent hippocampal neuronal dysfunction. *J Neurochem* 2011; 117: 100–111.
7. Ribeiro JA, Sebastião AM and de Mendonça A. Adenosine receptors in the nervous system: pathophysiological implications. *Prog Neurobiol* 2002; 68: 377–392.
8. Gomes CV, Kaster MP, Tomé AR, et al. Adenosine receptors and brain diseases: neuroprotection and neurodegeneration. *Biochim Biophys Acta* 2011; 1808: 1380–1399.
9. Fredholm BB, Chen JF, Cunha RA, et al. Adenosine and brain function. *Int Rev Neurobiol* 2005; 63: 191–270.
10. Dall'Igna OP, Porciúncula LO, Souza DO, et al. Neuroprotection by caffeine and adenosine A2A receptor blockade of beta-amyloid neurotoxicity. *Br J Pharmacol* 2003; 138: 1207–1209.
11. Blum D, Hourez R, Galas MC, et al. Adenosine receptors and Huntington's disease: implications for pathogenesis and therapeutics. *Lancet Neurol* 2003; 2: 366–374.
12. Cunha RA, Ferré S, Vaugeoi JM, et al. Potential therapeutic interest of adenosine A2A receptors in psychiatric disorders. *Curr Pharm Des* 2008; 14: 1512–1524.
13. Schwarzschild MA, Agnati L, Fuxe K, et al. Targeting adenosine A2A receptors in Parkinson's disease. *Trends Neurosci* 2006; 29: 647–654.
14. Varani K, Abbracchio MP, Cannella M, et al. Aberrant A2A receptor function in peripheral blood cells in Huntington's disease. *FASEB J* 2003; 17: 2148–2150.
15. Ishiwata K, Ogi N, Hayakawa N, et al. Adenosine A2A receptor imaging with [11C]KF18446 PET in the rat brain after quinolinic acid lesion: comparison with the dopamine receptor imaging. *Ann Nucl Med* 2002; 16: 467–475.

16. Mishina M, Ishiwata K, Naganawa M, et al. Adenosine A(2A) receptors measured with [11C]TMSX PET in the striata of Parkinson's disease patients. *PLoS One* 2011; 6: e17338.

17. Ramlackhansingh AF, Bose SK, Ahmed I, et al. Adenosine 2A receptor availability in dyskinetic and non-dyskinetic patients with Parkinson disease. *Neurology* 2011; 76: 1811–1816.

18. Barret O, Hannestad J, Vala C, et al. Characterization in humans of 18F-MNI-444, a PET radiotracer for brain adenosine 2A receptors. *J Nucl Med* 2015; 56: 586–591.

19. Naganawa M, Kimura Y, Mishina M, et al. Quantification of adenosine A2A receptors in the human brain using [11C]TMSX and positron emission tomography. *Eur J Nucl Med Mol Imaging* 2007; 34: 679–687.

20. Brooks DJ, Doder M, Osman S, et al. Positron emission tomography analysis of [11C]KW-6002 binding to human and rat adenosine A2A receptors in the brain. *Synapse* 2008; 62: 671–681.

21. Mishina M, Ishiwata K, Kimura Y, et al. Evaluation of distribution of adenosine A2A receptors in normal human brain measured with [11C]TMSX PET. *Synapse* 2007; 61: 778–784.

22. Naganawa M, Mishina M, Sakata M, et al. Test-retest variability of adenosine A2A binding in the human brain with 11C-TMSX and PET. *EJNMMI Res* 2014; 4: 76[aq].

23. Moresco RM, Todde S, Belloli S, et al. In vivo imaging of adenosine A2A receptors in rat and primate brain using [11C]SCH442416. *Eur J Nucl Med Mol Imaging* 2005; 32: 405–413.

24. Hirani E, Gillies J, Karasawa A, et al. Evaluation of [4-O-methyl-(11)C]KW-6002 as a potential PET ligand for mapping central adenosine A(2A) receptors in rats. *Synapse* 2001; 42: 164–176.

25. Ishiwata K, Noguchi J, Wakabayashi S, et al. 11C-labeled KF18446: a potential central nervous system adenosine A2a receptor ligand. *J Nucl Med* 2000; 41: 345–354.

26. Khanapur S, Paul S, Shah A, et al. Development of [18F]-labeled Pyrazolo [4, 3-e]-1, 2, 4-triazolo [1, 5-c] pyrimidine (SCH442416) analogs for the imaging of Cerebral Adenosine A2A receptors with Positron Emission Tomography. *J Med Chem* 2014; 57: 6765–6780.

27. Zhou X, Khanapur S, Huizing AP, et al. Synthesis and preclinical evaluation of 2-(2-furanyl)-7-[2-[4-[4-(2-[11C]methoxyethoxy)phenyl]-1-piperazinyl]ethyl]7H-pyr azolo[4,3-e][1,2,4]triazolo[1,5-c]pyrimidine-5-amine ([11C]Preladenant) as a PET tracer for the imaging of cerebral adenosine A2A receptors. *J Med Chem* 2014; 57: 9204–9210.

28. Cutler DL, Tendolkar A and Grachev ID. Safety, tolerability and pharmacokinetics after single and multiple doses of preladenant (SCH420814) administered in healthy subjects. *J Clin Pharm Ther* 2012; 37: 578–587.

29. Alfaro TM, Vigia E, Oliveira CR, et al. Effect of free radicals on adenosine A(2A) and dopamine D2 receptors in the striatum of young adult and aged rats. *Neurochem Int* 2004; 45: 733–738.

30. Leenders KL, Perani D, Lammertsma AA, et al. Cerebral blood flow, blood volume and oxygen utilization. Normal values and effect of age. *Brain* 1990; 113: 27–47.

31. Bazan NG, Braquet P and Ginsberg MD. Neurochemical correlates of cerebral ischemia. In: Ginsberg MD, Braquet P and Bazan (eds). *Introduction: Current biochemical and molecular approaches to the study of cerebral ischemia.* New York, NY: Plenum Press, 1992, pp.1–8.

32. Julien-Dolbec C, Tropres I, Montigon O, et al. Regional response of cerebral blood volume to graded hypoxic hypoxia in rat brain. *Br J Anaesth* 2002; 89: 287–293.

33. Innis RB, Cunningham VJ, Delforge J, et al. Consensus nomenclature for in vivo imaging of reversibly binding radioligands. *J Cereb Blood Flow Metab* 2007; 27: 1533–1539.

34. Fleiss J (ed.) The design and analysis of clinical experiments. In: *Reliability of measurement.* Danvers, MA: John Wiley & Sons, Inc, 1986, pp.1–32.

35. Shrout PE and Fleiss JL. Intraclass correlations: uses in assessing rater reliability. *Psychol Bull* 1979; 86: 420–428.

36. Parkinson FE and Fredholm BB. Autoradiographic evidence for G-protein coupled A2-receptors in rat neostriatum using [3H]-CGS 21680 as a ligand. *Naunyn Schmiedebergs Arch Pharmacol* 1990; 342: 85–89.

37. Shimada J, Koike N, Nonaka H, et al. Adenosine A$_{2A}$ antagonists with potent anti-cataleptic activity. *Bioorg Med Chem Lett* 1997; 7: 2349–2352.

38. Slifstein M and Laruelle M. Effects of statistical noise on graphic analysis of PET neuroreceptor studies. *J Nucl Med* 2000; 41: 2083–2088.

39. Buchert R, Varga J and Mester J. Limitations of bi-linear regression analysis for the determination of receptor occupancy with positron emission tomography. *Nucl Med Commun* 2004; 25: 451–459.

40. Lammertsma AA and Hume SP. Simplified reference tissue model for PET receptor studies. *Neuroimage* 1996; 4(3 Pt 1): 153–158.

41. Parsons B, Togasaki DM, Kassir S, et al. Neuroleptics up-regulate adenosine A2a receptors in rat striatum: implications for the mechanism and the treatment of tardive dyskinesia. *J Neurochem* 1995; 65: 2057–2064.

42. Barret O, Hannestad J, Alagille D, et al. Adenosine 2A receptor occupancy by tozadenant and preladenant in Rhesus monkeys. *J Nucl Med* 2014; 55: 1712–1718.